# **Nanoscale**



PAPER View Article Online
View Journal | View Issue



Cite this: Nanoscale, 2021, 13, 12521

# Improvement of alkali metal ion batteries *via* interlayer engineering of anodes: from graphite to graphene†

Jiachen Ma, (1) ‡a Chen Yang, (1) ‡a,b Xinjie Ma,c Shiqi Liu, (1) a Jie Yang,a Linqiang Xu,a Jingsong Gao,a Ruge Quhe,d Xiaotian Sun, (1) e Jinbo Yang,a,f,g,h Feng Pan, (1) i Xiaoyu Yang\*c,j,k and Jing Lu\*a,b,f,g,h

Interlayer engineering of graphite anodes in alkali metal ion (M = Li, Na, and K) batteries is carried out based on the first-principles calculations. By increasing the interlayer spacing of graphite, the specific capacity of Li or Na does not increase while that of K increases continuously (from 279 mA h  $g^{-1}$  at the equilibrium interlayer spacing to 1396 mA h  $g^{-1}$  at the interlayer spacing of 20.0 Å). As the interlayer spacing increases, the electrostatic potential of graphite becomes smoother, and the ability to buffer the electrostatic potential fluctuation becomes poorer in M ions. These two effects jointly lead to minima of the diffusion barrier of M ions on graphite (0.01–0.05 eV), instead of strictly monotonous declines with the increasing interlayer spacing. To perform the interlayer engineering of anode candidates more efficiently, a set of high-throughput programs has been developed and can be easily applied to other systems. Our research has guiding significance for achieving the optimal effect in interlayer engineering experimentally.

Received 28th March 2021, Accepted 24th June 2021 DOI: 10.1039/d1nr01946e

rsc.li/nanoscale

## Introduction

As the most significant energy storage devices in our daily life, the rechargeable alkali metal ion batteries have a strong performance dependence on electrode materials.<sup>1,2</sup> The typically used electrodes are composed of layered bulk materials, and we call them three-dimensional (3D) electrodes for short. They usually naturally exist or can be easily fabricated.<sup>3,4</sup> When the interlayer spacing of these layered materials is artificially expanded through interlayer engineering, they can transform into two-dimensional (2D) materials. The electrodes consisting of 2D materials, denoted as 2D electrodes for short, provide relatively larger specific surface,5,6 masses of electrochemically active sites, and ion storage space, which generally contribute to the large specific capacity further. 6-8 For example, from the anode with bulk C2N to its monolayer counterpart, the theoretical specific capacity increases from 705 mA h g<sup>-1</sup> to 2469 mA h  $g^{-1}$  for Li-ions, and from 470 mA h  $g^{-1}$  to 2939 mA h  $g^{-1}$  for Na-ions. 9,10 In the case of K-ion batteries, the experimental capacity increased by a factor of about 2.5 when the bulk graphite anode was changed to the 7 layers of the graphene anode.11

Besides, because the alkali metal ion on the surface of 2D materials experiences only half atom interaction compared with that in their bulk layered materials, it generally has a lower diffusion barrier and thus a faster charging–discharging rate.<sup>12</sup> For example, on replacing the bulk graphite anode with the 7 layers of the graphene anode in K-ion batteries, the rate capability is retained from almost zero to ~60% at the same current density of 3C experimentally.<sup>11</sup> The rate performance

<sup>&</sup>lt;sup>a</sup>State Key Laboratory for Mesoscopic Physics and Department of Physics, Peking University, Beijing 100871, P. R. China. E-mail: jinglu@pku.edu.cn <sup>b</sup>Academy for Advanced Interdisciplinary Studies, Peking University, Beijing 100871,

<sup>&</sup>quot;Academy for Advanced Interdisciplinary Studies, Peking University, Beijing 100871 P. R. China

<sup>&</sup>lt;sup>c</sup>Beijing MaiGao MatCloud Technology Co. Ltd, Beijing, 100190, P. R. China <sup>d</sup>State Key Laboratory of Information Photonics and Optical Communications and School of Science, Beijing University of Posts and Telecommunications, Beijing 100876, P. R. China

<sup>&</sup>lt;sup>e</sup>College of Chemistry and Chemical Engineering, and Henan Key Laboratory of Function-Oriented Porous Materials, Luoyang Normal University, Luoyang 471934, P. R. China

<sup>&</sup>lt;sup>f</sup>Collaborative Innovation Center of Quantum Matter, Beijing 100871, P. R. China <sup>g</sup>Beijing Key Laboratory for Magnetoelectric Materials and Devices, Beijing 100871, P. R. China

<sup>&</sup>lt;sup>h</sup>Peking University Yangtze Delta Institute of Optoelectronics, Nantong 226010, P. R. China

<sup>&</sup>lt;sup>i</sup>School of Advanced Materials, Peking University Shenzhen Graduate School, Shenzhen, 518055. P. R. China

<sup>&</sup>lt;sup>j</sup>Computer Network Information Centre, Chinese Academy of Sciences, Beijing, 100190, P. R. China. E-mail: kxy@cnic.cn

<sup>&</sup>lt;sup>k</sup>University of Chinese Academy of Sciences, Beijing, 100049, P. R. China

<sup>†</sup> Electronic supplementary information (ESI) available. See DOI: 10.1039/d1pr01946e

<sup>‡</sup>These authors contributed equally to this work.

with this few-layered graphite anode shows a critical improvement under the joint action of bulk diffusion and surface diffusion. 11 In the Li-ion batteries, the diffusion barrier is 0.34 eV when the Li-ion migrates within AA-stacked bilayer graphene, while it decreases to 0.26 eV on the outside under the same calculation setting. 13 Taken together, 2D electrodes are attracting more and more attention in recent years because of their contribution to battery capacity and rate performance.

The realistic 2D material electrode consists of substantial 2D materials. However, a free-standing individual 2D material is absent in the actual 2D electrode. Due to van der Waals interaction, these 2D materials tend to reaggregate into a mother layered bulk material.<sup>7,14</sup> In terms of doping, <sup>15–17</sup> functional group modification, 18 solvating/using complex anions, 19-23 assembling hierarchical architectures, 6,24-28 and so on, we can open the self-accumulated layered materials to some extent. Thus, the realistic 2D electrode can be simplified as a 3D layered material with an expanded interlayer spacing through interlayer engineering. Apparently, the electrode properties, such as specific capacity and diffusion barrier, depend on the interlayer spacing. Therefore, it is highly important to examine the electrode property dependence on the interlayer spacing of 3D layered materials and to find an overall optimal interlayer spacing.

In this work, we take the commercial-used 3D graphite anode and its 2D counterpart graphene anode in alkali metal ion batteries (M = Li, Na, and K) as examples (M/C systems for short) and investigate the dependence of the structural, energetic, electronic, and ionic features of the graphite anode on the interlayer spacing using density functional theory (DFT). The 3D graphite anode can gradually transform into the graphene anode by increasing the interlayer spacing. The term "interlayer spacing" is uniformly used for convenience. The initial specific capacity of the Li-graphite anode is 372 mA h  $g^{-1}$  and sharply drops to below 41 mA h  $g^{-1}$ , and then remains with the increasing interlayer spacing. The diffusion barrier of the Li-ion is 0.47 eV at the equilibrium interlayer spacing, and drops to the minimum of 0.05 eV, and rebounds to 0.30 eV with the increasing interlayer spacing. The initial specific capacity of the Na-graphite anode is below 35 mA h g<sup>-1</sup> at any interlayer spacing. The diffusion barrier of the Na-ion is 0.29 eV at its equilibrium interlayer spacing of 4.5 Å and decreases to a minimum of 0.01 eV and remains. The enlarged interlayer spacing has no contribution to the specific capacity in the Liion and Na-ion batteries. While for the K-graphite anode, the initial specific capacity continuously increases from 279 mA h  $g^{-1}$  at its equilibrium interlayer spacing of 5.4 Å to 1396 mA h g<sup>-1</sup> at an interlayer spacing of 20.0 Å. The diffusion barrier of the K-ion is 0.15 eV at 5.4 Å and decreases to a minimum of 0.01 eV, and then slightly rebounds to 0.05 eV. Besides, the working mechanism of the anodes shows a tendency from intercalation to plating with the increasing interlayer spacing in the K-ion batteries.

We find that interlayer engineering can indeed improve the performance of batteries. Thus, a strategy is put forward to choose an overall optimal interlayer spacing, according to the

performance of capacity, ion transfer, and electron transfer. Although different kinds of electrode hosts and ions show various features when the interlayer spacing changes, the research methods and procedures are the same. In order to investigate other electrodes more efficiently, we also develop a set of high-throughput (HT) computing programs, including the diffusion barrier calculation and capacity estimation. This set of HT computing programs can be easily applied to other systems in need.

## Model and method

All calculations are performed using the Vienna ab initio simulation package (VASP).<sup>29,30</sup> The exchange and correlation functional is the Perdew-Burke-Ernzerhof (PBE) form of the generalized gradient approximation (GGA). 31-34 The pseudopotential is projector augmented wave (PAW)35 with a high energy cutoff of 600 eV to ensure accuracy. The valence electrons for Li, C, Na, and K are  $2s^1$ ,  $2s^22p^2$ ,  $3s^1$ , and  $3s^23p^64s^1$ , respectively. The zero damping DFT-D3 method of Grimme36,37 is adopted according to the van der Waals correction test (details are given in part 1 in the ESI†). All structures are fully relaxed with the convergence threshold of 10<sup>-6</sup> eV in energy and 10<sup>-3</sup> eV  $\mathring{A}^{-1}$  in force. For graphite (C<sub>6</sub>) and stage-I graphite (M<sub>n</sub>C<sub>6</sub> and  $M_nC_8$ ) structures, the 7 × 7 × 7 Monkhorst-Pack k-point meshes in the Brillouin zone are set for geometry optimization and the 15  $\times$  15  $\times$  15 one for static electronic structure calculations. The term stage-I refers to the point when the M ions separate the anode host layers one by one. For stage-I graphite supercells (MC<sub>24</sub> and M<sub>x</sub>C<sub>54</sub>), the k-point meshes are set as 3  $\times$  $3 \times 3$  for geometry optimization and  $7 \times 7 \times 7$  for static electronic structure calculations. For the ion transport, the climbing-image nudged elastic band (CI-NEB) method38-41 is applied on MC24 supercells to find the diffusion path with minimum diffusion barriers. Three intermediate images are linearly inserted in each structure.

The high-performance calculations are designed and carried out on the MatCloud+ High Throughput Materials Simulation platform. 42,43 The initial structures and the calculation parameters of the conventional and the HT methods are the same.

## Results and discussion

## 3.1. Adsorption of a single layer of M ions

To begin with, we calculate the structural, energetic, electronic, and ionic properties of graphite adsorbing a single layer of M ions under different carbon interlayer spacings d and then analyze their evolution features. We use the most commonly studied stage-I structure, MC6, to investigate the first three properties. To further eliminate the influence of the M-M Coulomb repulsion, we use a larger supercell, MC<sub>24</sub>, to investigate the ionic properties. The AA-stacked carbon host is chosen since it is more energetically favorable than the AB-

Nanoscale Paper

stacked counterpart with one layer of M ions adsorbed. 13 d is set with an upper limit of 20 Å, which is large enough to model the graphene anode.

For the structural properties, we illustrate the vertical distance  $d_i$  (i = 1, 2) between the M ion layer and the two adjacent carbon layers under different d in Fig. 1(a). In the stage-I structure of this work, each M ion is sandwiched between two carbon layers.  $d_1$  (or  $d_2$ ) refers to the vertical distance between the M ion and the closer (or further) carbon layer. We have  $d = d_1 + d_2$ . The tendencies of  $d_1$  or  $d_2$  for Li, Na, and K ions with the increasing interlayer spacing are similar: when dis smaller than a threshold value  $d_{th}$ ,  $d_1 = d_2 = d/2$ ; when d > d $d_{\rm th}$ ,  $d_1 < d_2$ . After the threshold,  $d_1$  has a small decline (LiC<sub>6</sub>,  $NaC_6$ ) or wave (KC<sub>6</sub>) and then stays constant, while  $d_2$  keeps increasing.

Quantificationally,  $d_{th}$  of the LiC<sub>6</sub>, NaC<sub>6</sub>, and KC<sub>6</sub> structures are 4.0, 8.0, and 7.0 Å, respectively. When  $d > d_{th}$  for each,  $d_1$ of LiC<sub>6</sub> drops by 0.2 Å and is stabilized at 1.8 Å, and  $d_1$  of NaC<sub>6</sub> drops by 0.5 Å and is stabilized at 3.5 Å. Unlike the case of  $LiC_6$  and  $NaC_6$ ,  $d_1$  of  $KC_6$  increases by 0.1 Å when d reaches 8.0 Å, and then drops by 0.3 Å and stabilizes at 3.3 Å. By changing d, the LiC<sub>6</sub>, NaC<sub>6</sub>, and KC<sub>6</sub> structures have the largest  $d_{1\text{max}}$  of 2.0, 4.0, and 3.6 Å, respectively. It can be speculated that the abnormal decline or wave of  $d_1$  after the threshold is caused by the attraction of the further carbon layer to the M ion, which makes the ion stay relatively away from the closer one. Since this intensity of attraction is inversely related to the value of  $d_2$ ,  $d_1$  tends to be only affected by the closer carbon layer and stabilized when d is rather large. The large  $d_1$  is conducive to the low ionic diffusion barrier and will be elaborated

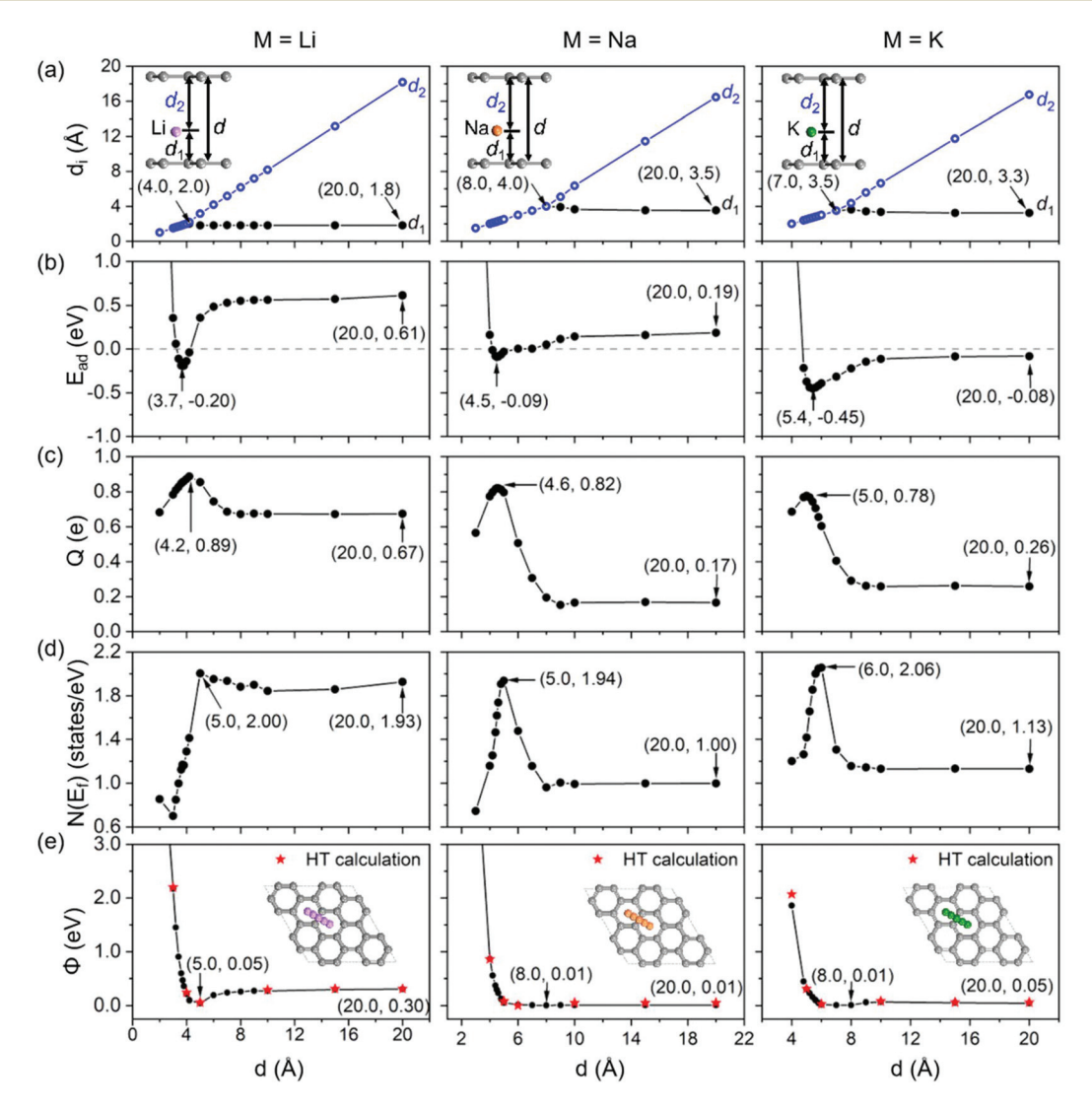


Fig. 1 (a) Vertical distance (d<sub>i</sub>) between the M ion layer and the adjacent two carbon layers, (b) adsorption energy ( $E_{ad}$ ), (c) transferred electrons (Q) from the M atom to the carbon layers, and (d) the density of states at  $E_f(N(E_f))$  per MC<sub>6</sub> unit cell at different interlayer spacings d. (e) Diffusion barriers  $(\Phi)$  of the M ion migrating parallel to the graphene planes  $(MC_{24})$  at different d values. The migrating pathways are depicted in the illustration. M represents Li, Na, and K from left to right. The data represented by the red pentagrams are obtained by the HT program, which generally coincide with the traditional calculated ones. More data are calculated when the properties change more drastically with the interlayer spacing.

later in the ionic property part of this section. Besides, it is worth noting that  $d_{th}$  and steady  $d_1$  are both in the sequence of Li < K < Na, which are different from Shannon's ionic radii in the Li < Na < K sequence with the same coordinate number of VI. 44,45 This inverted order between Na and K is thought to be related to their actual charge transfer situation, namely the real ionic radii in the anode environment.<sup>45</sup> The analysis of the inverted order will also be given later in the electronic property part of this section.

Based on the previous studies, the adsorption energy  $(E_{ad})$ can be measured as follows:46

$$E_{\rm ad} = E_{\rm MC_6} - E_{\rm C_6} - E_{\rm M} \tag{1}$$

where  $E_{MC_6}$  and  $E_{C_6}$  are the total energies of MC<sub>6</sub> and C<sub>6</sub> at the set interlayer spacing, respectively.  $E_{\rm M}$  is the total energy per M atom in its bulk structure. The negative  $E_{ad}$  means the adsorption is exothermic and spontaneous. As shown in Fig. 1(b), the interlayer spacings  $d_{eq}$  of the most stable state are 3.7, 4.5, and 5.4 Å for the LiC<sub>6</sub>, NaC<sub>6</sub>, and KC<sub>6</sub> structures, respectively. Given  $d_{\rm eq}$  of 3.66 Å under the AA-stacked mode and 3.42 Å under the AB-stacked mode for pristine graphite, the singlelayer M ions enlarge the interlayer spacing of graphite. The total energies of pristine graphite at different d are given in part 2 of the ESI.†

The  $E_{\rm ad}$  of Li, Na, and K ions all plummet first with the increasing d and then increase slowly until they reach constant values. For the LiC<sub>6</sub> structure,  $E_{\rm ad}$  is -0.20 eV per Li-ion at  $d_{\rm eq}$ = 3.7 Å, which is consistent with the previous theoretical result of -0.21 eV per Li-ion.<sup>47</sup> The  $E_{\rm ad}$  of LiC<sub>6</sub> is negative for 3.3 < d< 4.2 Å. As d increases,  $E_{\rm ad}$  increases to 0.61 eV per Li-ion when d = 7.0 Å and then remains constant. This value of  $E_{ad}$  is consistent with the previous DFT results of about 0.6 eV per Liion on graphene. 48 The final positive  $E_{ad}$  manifests that graphene cannot spontaneously adsorb Li-ions, implying a low theoretical capacity of the graphene anode in the Li-ion batteries.

For the NaC<sub>6</sub> structure,  $E_{\rm ad}$  is -0.09 eV per Na-ion at  $d_{\rm eq}$  = 4.5 Å, which is consistent with the previous theoretical result of about -0.1 eV per Na-ion. When 4.2 < d < 5.0 Å,  $E_{ad}$  is technically negative but pretty close to 0. When d > 10 Å,  $E_{ad}$ almost stays constant with a value of 0.19 eV per Na-ion. These high  $E_{\rm ad}$  indicate the poor capacity performance in the Na/C system at any interlayer spacing.

For the  $KC_6$  structure,  $E_{ad}$  reaches its minimum of -0.45 eV per K-ion at  $d_{eq}$  = 5.4 Å, which is consistent with the previous theoretical result of -0.48 eV per K-ion. <sup>50</sup>  $E_{\rm ad}$  remains negative when d > 4.7 Å. Until d > 10.0 Å,  $E_{ad}$  hardly changes with a value of -0.08 eV per Na-ion. The persistent negative  $E_{ad}$  forecasts a great K-ion capacity of both the graphite and graphene anodes. Besides, compared with the Li-ion, the K-ion has more negative  $E_{ad}$  with both graphite and graphene hosts, which indicates that the K-ion has a stronger bonding and better wetting performance with the carbon host. A better wetting means the electrode host has a larger contact area with the metal ions and corresponds to lower interfacial resistance.<sup>51</sup>

The origin of the wetting difference between Li and K with carbon host deserves deeper study.

The enlarged  $d_{eq}$  compared with pristine graphite implies the volume changes during the charging-discharging process if the graphite anode has no modification, especially in the Na-ion and K-ion batteries. Nevertheless, the most negative  $E_{ad}$ for the three MC<sub>6</sub> structures still occur when the carbon layers are at their bulk state, manifesting that the 3D graphite anode has a stronger adsorption ability to M ions than the graphene anode. The much higher  $E_{ad}$  in LiC<sub>6</sub>, NaC<sub>6</sub>, and KC<sub>6</sub> at d =20 Å manifest the relatively poor wetting of graphene with the alkali metals.51

For the electronic properties, the number of the transferred electrons from M atoms to carbon layers (Q) and the density of states at the Fermi levels  $(N(E_f))$  are further calculated. The larger Q indicates the stronger ionic bonding between the carbon host and the M ions, and the smaller ionic radius for the same element. In Fig. 1(c), the maxima of Q in LiC<sub>6</sub>, NaC<sub>6</sub>, and KC<sub>6</sub> structures are 0.89, 0.82, and 0.78 e per M atom at a d of 4.2, 4.6, and 5.0 Å, respectively, which are almost the same with those at their  $d_{eq}$  (0.86, 0.82, and 0.74 e for per M atom in  $LiC_6$ ,  $NaC_6$ , and  $KC_6$  structures, respectively). When d reaches a certain value (LiC<sub>6</sub>: 7 Å; NaC<sub>6</sub>: 10 Å; KC<sub>6</sub>: 10 Å), Q remains constant instead of decreasing. When d = 20 Å, Q are 0.67, 0.17, and 0.26 e per M atom in LiC<sub>6</sub>, NaC<sub>6</sub>, and KC<sub>6</sub> structures, respectively. In general, we can find that M atoms transfer more electrons to graphite than to graphene. The phenomenon that Q remains relatively large from the Li atom to graphene but rather small from Na, or K atom to graphene deserves to be further studied. Moreover, the K atom transfers more electrons than the Na atom at the same d > 5 Å. So the real ionic radius for K is closer to Shannon's one, while the real ionic radius for Na may be much larger than Shannon's one. It can explain the inverted order of interlayer spacing thresholds between Na and K. Besides, compared with the trend of the adsorption energy, a larger Q roughly corresponds to a more negative  $E_{ad}$  for each element, indicating that the proportion of ionic bonds may have a great impact on the adsorption energy.

According to the Einstein relation  $\sigma = e^2 \frac{\mathrm{d}n}{\mathrm{d}\mu} D_{\mathrm{diff}}$ , the electronic conductivity  $\sigma$  is positively correlated to the electronic density of states at the Fermi level  $\frac{dn}{d\mu} = N(E_f)$ , where  $D_{\text{diff}}$  is the diffusion constant.  $^{52}$   $N(E_{\rm f})$  are 1.17, 1.62, and 1.85 states per eV for LiC<sub>6</sub>, NaC<sub>6</sub>, and KC<sub>6</sub> unit cells at their  $d_{eq}$ , respectively. For the  $LiC_6$  unit cell,  $N(E_f)$  increases from 0.70 states per eV at d = 3 Å to 2.00 states per eV at d = 5 Å and then keeps within 1.84–2.00 states per eV. At d = 20 Å,  $N(E_f)$  for the LiC<sub>6</sub> unit cell is 1.93 states per eV. The abnormally high  $N(E_f)$  of the  $LiC_6$  structure at d = 2 Å is caused by the band structure deformation with the extremely small interlayer spacing, and the detailed analysis is given in part 3 of the ESI.† For the Na and K counterparts,  $N(E_f)$  has a summit of 1.94 states per eV at d =5 Å and 2.06 states per eV at d = 6 Å but drops to 1.00 and 1.13 states per eV at d = 20 Å per unit cell, respectively. Similar to Q,  $N(E_{\rm f})$  also stays large for the Li-ion but decreases drastically for

Nanoscale

the Na- and K-ion from the graphite anode to the graphene anode. The persistent high Q and  $N(E_{\rm f})$  for the Li-ion both manifest that the anode with Li-ions can retain fast electronic conduction when the spacing of carbon layers increases. However, the falls of Q and  $N(E_{\rm f})$  for the Na- and K-ion imply the underlying poorer electronic-conducting performance from the graphite anode to the graphene anodes in the Na-ion and K-ion batteries.

For the ionic properties, the CI-NEB method is specially performed. As shown in Fig. 1(e), in general, the diffusion barriers  $(\Phi)$  fall drastically and then remain still for all alkali metal ions. Energy profiles are provided as Fig. S4.† Their energetically favorable  $d_{eq}$  is 3.8, 4.4, and 5.4 Å for LiC<sub>24</sub>, NaC<sub>24</sub>, and  $KC_{24}$ , respectively, and the corresponding  $\Phi_{eq}$  are 0.36, 0.37, and 0.15 eV. d with the lowest barriers for LiC<sub>24</sub>, NaC<sub>24</sub>, and KC<sub>24</sub> are 5.0, 8.0, and 8.0 Å, respectively, and the corresponding  $\Phi_{\min}$  are 0.05, 0.01, and 0.01 eV, respectively. The above data show that the enlarged interlayer spacing can markedly reduce the ion diffusion barriers. When the interlayer spacing d continuously increases,  $\Phi$  finally stabilizes at 0.30, 0.01, and 0.05 eV for LiC24, NaC24, and KC24, respectively, which is also consistent with the previous theoretical studies (0.311,<sup>53</sup> 0.096,<sup>54</sup> and 0.039 eV (ref. 55) for Li-, Na-, and K-ions on pristine graphene supercells). It is interesting that the barrier has a little pit near its minimum, rather than strictly monotonically descending. Besides, it also shows a strong dependence between the d of  $\Phi_{\min}$  and the d of  $d_{1\max}$ . Given that, we illustrate the electrostatic potential for carbon layers (U) along the x-axis at the different interlayer spacing in Fig. 2. From graphite to graphene, U becomes smoother and smoother, leading to the overall decrease in  $\Phi$ . Focusing on d around  $\Phi_{\min}$ ,  $d_1$  and  $\Delta d_1$  for MC<sub>24</sub> during M ion diffusion are listed in Table 1.  $d_1$  can reflect the degree of in-plane fluctuation of U, and  $\Delta d_1$  can reflect the ability of M ions to buffer

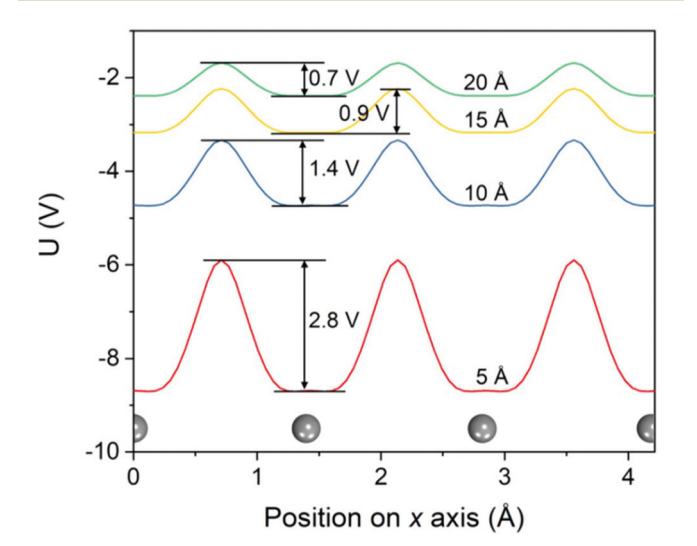


Fig. 2 Electrostatic potential of the AA-stacked carbon layers (U) along the x-axis, namely parallel to the carbon layers. The interlayer spacing between carbon layers is set as 5, 10, 15, and 20 Å, respectively. The positions of C atoms along the x-axis are marked with gray spheres.

**Table 1** Structural details of  $MC_{24}$  (M = Li, Na, and K) at the interlayer spacing near the barrier minimum. From the top view, the M ion migrates from the center of a carbon ring (hollow site, H for short), over the C–C bond (bridge site, B for short), to the center of the neighboring carbon ring during the CI-NEB calculation.  $d_1$  represents the vertical distance between the M ion and its nearest carbon layer.  $\Delta d_1$  refers to the  $d_1$  difference between the H site and B site

Structures	Interlayer spacing (Å)	$d_1$ (Å)			
		H site	B site	$\Delta d_1  (\mathring{\mathrm{A}})$	
LiC <sub>24</sub>	4	1.9996	2.0007	0.0011	
	5	1.8332	2.2943	0.4611	
	6	1.7391	2.0228	0.2837	
NaC <sub>24</sub>	7	3.4942	3.4935	-0.0007	
	8	3.3768	3.3905	0.0137	
	9	3.2809	3.2931	0.0122	
$KC_{24}$	7	3.4947	3.4942	-0.0005	
	8	3.9944	3.9964	0.0020	
	9	2.5926	2.6902	0.0976	

the fluctuation of U by changing its vertical distance to the closer carbon layer during diffusion. It can be found that  $\Phi_{\min}$  appears when either  $d_1$  is relatively large (LiC<sub>24</sub>, NaC<sub>24</sub>) or  $\Delta d_1$  is large (KC<sub>24</sub>). These data show that the value of  $\Phi$  is the joint result of the degree of the fluctuation of U and the ability of M to buffer the fluctuation of U. When  $\Phi$  no longer changes with d, it can be considered that the M ion has large enough space to buffer the potential fluctuation and the diffusion of the M ion is only influenced by the closer carbon layer. In other words, the ion-transfer mechanism changes from bulk diffusion to surface diffusion, which is conducive to improving rate performance. This also explains why the amplitude of electrostatic potential fluctuation of expanded graphite has a difference of 0.2 eV under d=15 Å and 20 Å, while the diffusion barriers are the same for each M ion.

## 3.2. Adsorption of multiple layers of M ions

To investigate the dependence of adsorption of multiple layers of M ions on the interlayer spacing, we measure the specific capacity as follows:<sup>57,58</sup>

$$C = \frac{x_{\text{max}}zF}{W} \tag{2}$$

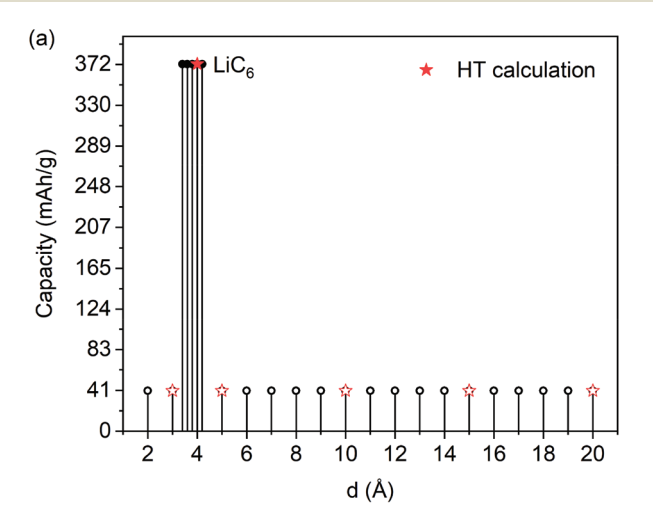
where W,  $x_{\rm max}$ , z, and F are the relative molecular mass of the graphite anode at the set d in g mol<sup>-1</sup>, the maximum adsorption concentration of M ions, the valence number (z = 1 for Li, Na, and K), and the Faraday constant (26810 mA h mol<sup>-1</sup>), respectively. For the selected anode materials (graphite) and ionic carriers (Li, Na, and K), the specific capacity is simply determined by  $x_{\rm max}$ , which will change with d.  $x_{\rm max}$  can be measured by the average adsorption energy ( $E_{\rm ave}$ ) and the open-circuit voltage (OCV) with the formulas: <sup>57,58</sup>

$$E_{\text{ave}} = \frac{E_{\text{MxC}} - E_{\text{C}} - xE_{\text{M}}}{x} \tag{3}$$

$$OCV = \frac{E_{M_{x_2}C} - E_{M_{x_1}C} - (x_2 - x_1)E_{M_{x_2}C}}{(x_2 - x_1)e}$$
(4)

where  $E_{MxC}$ ,  $E_{M_{x_1}C}$ , and  $E_{M_{x_2}C}$  are the total energies of the M ion adsorbed graphite anode at the set d with an M ion concentration of x,  $x_1$ , and  $x_2$ , respectively.  $E_C$  and  $E_M$  are the total energies of the graphite anode at the set interlayer spacing and per M atom in its bulk structure. The negative  $E_{ave}$  value represents that the overall adsorption process is spontaneous exothermic, and the positive OCV value manifests that the new coming M tends to be adsorbed in terms of ionic states rather than metallic states, or vice versa. With the increasing concentration, the Coulomb repulsion among M ions becomes more vigorous, leading to an increase of  $E_{ave}$  and a decrease of OCV.  $^{7,58,59}$  When either  $E_{ave}$  becomes positive or OCV becomes negative, the adsorption concentration reaches its maximum value,  $x_{\text{max}}$ . Details of  $E_{\text{ave}}$  and OCV are given in part 5 of the

According to the results of  $E_{ave}$  and OCV, the calculated specific capacity for the Li-ion or K-ion adsorbed carbon layer at different d is illustrated in Fig. 3. In order to get a more



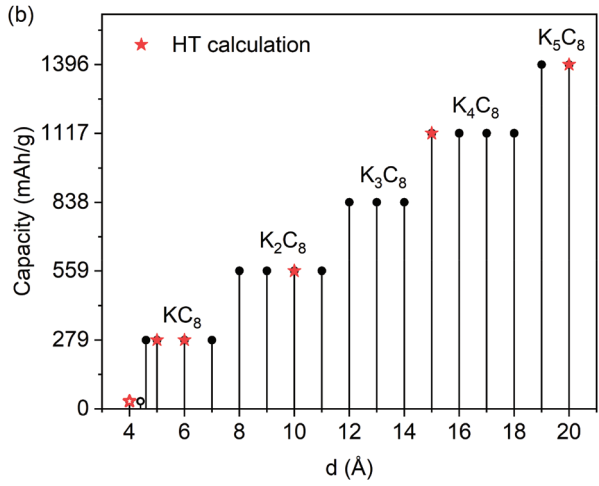


Fig. 3 Capacity of the carbon layers at different d values of (a) Li and (b) K according to  $E_{ave}$  and OCV. The hollow circles or pentacles indicate that the corresponding capacity values are not reached. The data represented by the red pentacles are obtained by the HT program, which coincide with the traditional calculated ones.

accurate critical point of the capacity changing from negligible small to having a substantial value, a denser interlayer spacing sampling is adopted around the critical point. For the Li-ion, the carbon anode only possesses a substantial capacity of 372 mA h g<sup>-1</sup> (LiC<sub>6</sub>) when 3.3 < d < 4.2 Å. Such a capacity is consistent with that in the bulk pristine graphite anode for Liion batteries in experiments (370–380 mA h  $g^{-1}$ ). <sup>56,60</sup> When d <3.3 Å, the strong Coulomb repulsion among C and Li atoms inhibits the Li intercalation. When d > 4.2 Å, the bonding between the Li-ion and the carbon host is too weak to fix the Li-ions. Thus,  $E_{\text{ave}}$  becomes positive after 4.2 Å even at a low concentration of x = 1/54 (LiC<sub>54</sub>), which corresponds to an unreached capacity of 41 mA h g<sup>-1</sup>. However, few-layered graphene can hold a large Li-ion capacity in experiments. For example, Sonia et al. found that the Li-ion capacity of the fewlayered graphene (~7 layers) anode is about 3-4 times that of the bulk graphite (~450 nm thick) anode. 56 The large Li-ion capacity of graphene is mainly contributed by the "stepped edges" of graphene, which has been verified both theoretically and experimentally.56 Other defects, such as the domain/grain boundaries of alternate pentagon-heptagon pairs or Stone-Wales defects and divacancies can also increase the storage of Li-ions but has non-negligible contribution only when they have large defect concentration.61-64

Regarding the Na-ion, the previous studies show that its specific capacity with the pristine graphite anode is below 35 mA h  $g^{-1}$  (corresponds to NaC<sub>64</sub>) both theoretically and experimentally, 49,65-67 which is too small for practical use. The DFT studies find that Na has relatively weaker ionic and covalent co-bonding with C compared with other alkali metal ions<sup>68</sup> and the Na-intercalation stretches the C-C bonds.<sup>49</sup> With the help of ether-based electrolytes, the expanded graphite can store Na-ions with a capacity of 150-220 mA h g<sup>-1</sup>.20,69,70 These solvent molecules can not only enlarge the spacing of graphite but also screen the bad interaction between Na and C. 19,21,22 Whereas, only enlarging the interlayer spacing cannot enhance the capacity performance since graphene even has weaker bonding with Na than graphite. In the experiment, the number of Na-ions adsorbed/desorbed on single-layered graphene reversibly without the ether-based electrolyte is lower than 20 µA h cm<sup>-2</sup>, which is further confirmed to be the electrochemical response of the copper substrate, rather than that of the graphene anode. 71 Besides, we calculated that  $E_{\text{ave}}$  of stage-I NaC<sub>6</sub> and NaC<sub>8</sub> configurations are rather high at any interlayer spacing of graphite ( $E_{ave}$  > -0.09 eV per Na-ion, shown in part 6 of the ESI†), which will lead to a rather small capacity. Thus, we do not take the multiadsorption performance of Na on graphite/graphene into account.

Unlike the case of Li-ions and Na-ions, the capacity of K-ions increases continuously with the increasing interlayer spacing. At first, the capacity is below 31 mA h  $g^{-1}$  (KC<sub>72</sub>) when d < 4.6 Å, due to the strong Coulomb repulsion. When 4.6 Å < d < 7.0 Å, it has a substantial theoretical capacity of 279 mA h g<sup>-1</sup> (KC<sub>8</sub>), which is consistent with the experimental value of the pristine graphite anode (273 mA h

Nanoscale  $g^{-1}$ ). Compared with the bulk graphite anode (about 1400 (a)  $g^{-1}$ ).

g<sup>-1</sup>).<sup>72</sup> Compared with the bulk graphite anode (about 1400 carbon layers), the capacity of the 7-layered graphene anode in the K-ion battery increases to about 2.5 times in experiments, and the capacity increases as the number of graphene layers decreases (~3 times for bilayer graphene).11 (One should distinguish the inner and outer interlayer spacing, details are shown in part 7 of the ESI.†) After K-ions intercalate into the spacing of graphene layers to form the KC8 structure, their DFT calculation shows that K-ions preferentially form a second layer on the few-layered graphene surface, and then accumulate at the edges. 11 The reason for the difference of adsorption priority between Liand K-ions on graphene deserves further study. According to our calculations, the graphite anode also shows an increasing K-ion capacity with the increasing interlayer spacing and the capacity is 1396 mA h  $g^{-1}$  (K<sub>5</sub>C<sub>8</sub>) at d = 20 Å. Under this circumstance, each carbon layer can adsorb five layers of K-ions. The energetically favorable adsorption of multilayered K-ions manifests that K can grow layer by layer, instead of forming dendrites like Li.51 This implies that K may be suitable for designing metal batteries.

In order to study the electronic properties of the multilayer adsorbed K-ions and find out whether there is an upper limit of the K-ion capacity with the increasing d, we further perform the Bader charge analysis and electron localization function (ELF) at d = 20 Å. As shown in Fig. 4(a), the total transferred charges (the total Q) from K atoms to carbon tend to increase with the increasing K layers. However, only when the newlyformed K layer adsorbs on the carbon layer the total Q increases obviously ( $C_8 \rightarrow KC_8$ ,  $K_2C_8 \rightarrow K_3C_8$ , and  $K_4C_8 \rightarrow K_5C_8$ ), and when the newly-formed K layer adsorbs on the K layer, the total Q remains almost unchanged (KC<sub>8</sub>→K<sub>2</sub>C<sub>8</sub>) or even decreases  $(K_3C_8 \rightarrow K_4C_8)$ . For example, the total Q stays almost the same from one layer of K adsorbed (0.29 e per KC8 unit cell) to two layers of K adsorbed (0.30 e per K<sub>2</sub>C<sub>8</sub> unit cell), but it increases to 0.69 e per K<sub>3</sub>C<sub>8</sub> unit cell with three layers of K-ions adsorbed. We find that the K<sub>4</sub>C<sub>8</sub> has a larger vertical distance between the carbon layer and its nearest K-ion layer than that of K<sub>3</sub>C<sub>8</sub>, which may explain the abnormal decrease of total Q here. The Q of each layer of K when K increases from one layer to five is shown in the right of Fig. 4(a). The K atoms near the carbon layer give more charge, while those far away from the carbon layer are almost neutral or even gain electrons.

The dependence of *Q* on the K-ion layer number is also reflected in ELF. As shown in Fig. 4(b), when there is only one layer of K on each side of the carbon layer (KC<sub>8</sub> and K<sub>3</sub>C<sub>8</sub>), the electrons of K are more localized. When there are two or more layers of K on one side of the carbon layer, these K contribute electrons forming free electron gas. These data indicate that the adsorbed K in multiple layers away from carbon layers tend to become metallic,<sup>73</sup> which is undesirable in ion batteries but normal in metal batteries. The working mechanism of the graphene anode gradually transforms from K intercalation to K plating as the number of adsorption layers increases. Thus, we cannot tell the upper limit of the storage capacity of

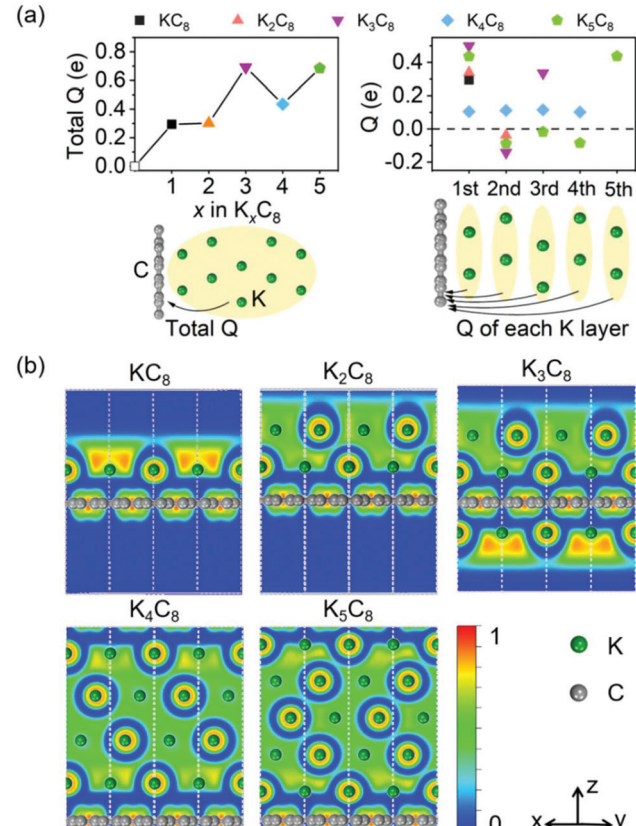


Fig. 4 (a) Transferred electrons (Q) from the K atoms to the C layer and (b) electron localization function (ELF) of  $K_xC_8$  (x=1,2,3,4, and 5) at the interlayer spacing of 20 Å. ELF is measured under the absolute scale with "1" representing the highest degree of electronic localization and "0" representing the lowest one.

K-ions since K-ions can keep plating on the carbon layered anode. More details can be seen in part 8 of the ESI.†

The above capacities are gained with the fixed *d* of graphite. With the limited d, K-ions cannot intercalate into the graphite anode without an end due to the increasingly strong Coulomb repulsion. Whereas, the strong Coulomb repulsion can be relieved if the lattice of K-intercalated graphite is allowed to change freely. Thus, we fully relax the lattice of  $K_xC_8$  structures and examine whether the graphite anode can adsorb multiple layers of K-ions without external pressure. In terms of  $E_{ave}$  and OCV, the adsorption of multiple K-ion layers is actually energetically feasible for the graphite anode in the ideal environment without any external stress. However, the equilibrium interlayer spacing  $d_{eq}$  of graphite, as a representative parameter of the lattice, changes drastically with K-ion intercalation/deintercalation. Compared with that of pristine AB-stacked graphite (3.42 Å),  $d_{eq}$  enlarges to 154% with one layer of K-ion (KC<sub>8</sub>) and 271% with two layers of K-ion (K<sub>2</sub>C<sub>8</sub>). Such huge volume changes are unacceptable in the actual scenarios. We also speculate that the reason why the graphite anode only holds a K-ion storage capacity of 273 mA h  $g^{-1}$  ( $\sim$ KC<sub>8</sub>) in practice<sup>72</sup> is that the anode would feel external pressure inevitably. Hence, interlayer engineering is still needed to enlarge the interlayer

spacing of the graphite anode at the very beginning to avoid the huge volume change. More details are given in part 9 of the ESI.†

## 3.3. Strategies for selecting the optimal interlayer spacing

Based on the above theoretical results, we can find that the properties of the graphite anode do not change strictly monotonically with the interlayer spacing d, and d is not always the bigger, the better. Besides, each property does not always perform the best at the same d. Thus, during interlayer engineering, it is necessary to consider various indicators comprehensively according to the designing needs and find out the overall optimal interlayer spacing  $d_{op}$ .

Given that the ion battery is an energy storage device essentially, we reckon that the first step is to ensure a substantial capacity with the selected interlayer spacing. Then, since ions move much slower than electrons, and the ion transport speed has a more obvious limiting effect on battery rate performance, the high ionic conductivity should be given priority over the high electronic conductivity.<sup>74</sup> Under conditions of high ionic conductivity, we can choose the interlayer spacing with higher electronic conductivity.

We perform the above strategies on the alkali metal ion batteries with the graphite anodes and try to find the  $d_{\mathrm{op}}$  of graphite. Regarding the Li-ion battery,  $d_{\rm op}$  should be designed at 3.3-4.2 Å to ensure a substantial capacity. Within this range, the Li-ion diffusion barrier becomes significantly smaller when d increases. Thus, the  $d_{op}$  of the graphite anode in the Li-ion battery is 4.2 Å. Regarding the Na-ion battery, we fail to find its  $d_{\rm op}$  when graphite is used as the anode, but the strategy and process of finding the optimal d are the same when other anode materials are considered. Regarding the K-ion battery, d should be larger than 4.7 Å to ensure substantial capacity. Within this range, the K-ion diffusion barrier is smallest when d = 8.0 Å and remains small when d > 6.0 Å. When d > 6.0 Å, the electronic transport slows down with the increase of d, and the electronic conductivity at 6.0 Å is much higher than that at 8.0 Å. Thus, the  $d_{\rm op}$  of the graphite anode is 8.0 Å in the K-ion battery. However, if the K battery is designed as a metal one, a larger  $d_{op}$ can also be considered due to the increasing specific capacity.

In the actual case, the electrochemical performance of the electrode is jointly influenced by d and the chosen interlayer engineering techniques. For example, the doping atoms not only enlarge the d of the electrode, but also provide extra active sites generally. Thus, to get  $d_{op}$  in the actual case, one should test the dependence of the electrochemical performance of the electrode on d with the specific interlayer engineering technique. Noticeably, the approaches and procedures are the same.

#### 4. Discussion

## 4.1. The high-throughput computing program for interlayer spacing engineering

To investigate the interlayer engineering performance of other layered electrode materials more efficiently, we have developed

a high-throughput computing program. Considering that the ion diffusion barrier calculation by the CI-NEB method and the ion storage capacity calculation are two of the most complicated tasks in analyzing the properties of anode materials, this HT program focuses on the automatic implementation of these two tasks. The flowchart is shown in Fig. 5.

The HT program firstly obtains the initial structures from databases. Then these structures are uniformly designed according to the needs like changing the interlayer spacing in this research (other modifications, such as doping or adding chemical groups, can also be achieved in a similar manner). All non-equivalent adsorption sites are found according to their symmetry, and the most stable adsorption site can be found by searching for the lowest adsorption energy. In the CI-NEB calculation part, the program will build supercells to avoid the Coulomb repulsion among the moving ions. In the initial and final images, the ions are set in the two nearest equivalent most stable sites by the CI-NEB method, respectively. Then the program screens the anode materials with a diffusion barrier that is smaller than the set value. The batteries made of these materials as anodes are expected to have good rate performance.

In the capacity calculation part, the program automatically finds the multiple M ion adsorbed structures with the lowest energy at each concentration of M until the maximum concentration is reached. Here the criteria for reaching the maximum concentration are that (1)  $E_{ave}$  becomes positive, or (2) OCV becomes negative, or (3) obvious structure deformation appears. 46,57,75,76 It is worth noting that the deformation criterion for graphite/graphene is usually not considered due to their high mechanical strength. However, some other materials may undergo larger deformations during the ion intercalation/deintercalation.75 Thus, the HT program considers the deformation criterion uniformly. After the maximum adsorption concentration is determined, the specific capacity is calculated. This HT program is specially designed for interlayer engineering and is expected to be used widely for other layered electrode materials.

## 4.2. Potential methods to perform interlayer spacing engineering

In experiments, interlayer engineering has four main approaches - doping, functional group modification, solvating or using complex anions, and assembling hierarchical architectures. As listed in Table 2, different methods extend the interlayer spacing of electrode materials to different degrees.

First, doping the electrode with larger radius atoms can slightly expand the interlayer spacing of electrode materials. N, P, and S atoms are usually used to replace C atoms. 16,17,77 The degree of expansion by doping is related to the atom radius difference and the interlayer spacing will not expand to exceed 0.1 nm in this way.

Second, the functional group modification approach refers to adding functional groups to the electrode host and thus enlarging the interlayer spacing. The degree of expansion by functional group modification is related to the types and

Obtain structures Capacity calculation **NEB** calculation Change interlayer Generate the initial spacing Adsorb more ions and final structures Search for possible high symmetric Calculate Optimize structures adsorption sites Eave/OCV/structure deformation Optimize structures CI-NEB calculations Calculate specific Find the most stable capacity Obtain diffusion adsorption site barriers for ions Analyze structure Calculate and Analyze ion and energetic analyze other behaviors behaviors properties

Nanoscale Paper

Fig. 5 Flowchart of the HT calculations of the anode materials properties. The diffusion barrier calculation (the orange area) and the capacity estimation (the blue area) are included.

Screen electrode materials

Table 2 Comparison of expansion of interlayer spacing in different experimental methods

General methods	Intrinsic electrode materials	Specific methods	Intrinsic interlayer spacing (nm)	Expanded interlayer spacing (nm)	Ref.
Doping	Graphite	N-Doping	0.335	0.344	16
	Graphite	S-Doping	_	0.38 - 0.41	17
	Hard carbon nanofibers	P-Doping	0.374	0.383	77
	MoSe <sub>2</sub>	N,P-Doping	0.62 - 0.65	0.68	81
Functional group	Graphite	C-OH and C=O groups	0.34	0.365-0.371	82
modification	Graphite	C-OH groups	0.34	0.43	18
	Multiwalled carbon nanotubes	C=O, $CH_x$ , C-OH, C-O-C, and O-C=O groups	0.37	<0.8	83
Solvating/using complex	Graphite	$AlCl_4^-$	_	0.57	84
anions	Graphite	[Na-DEGDME] + complex two [Na-DEGDME] + complexes	0.335	0.743 1.198	19
	$MoS_2$	Poly(ethylene oxide)	0.62	1.45	85
Hierarchical	$SnS_2$	SnS <sub>2</sub> /graphene/SnS <sub>2</sub> heterostructure	0.28 - 0.32	0.803	25
architectures	$MoS_2$	N-Doped graphene/MoS <sub>2</sub> heterostructure	0.62	0.99	86
	$MoS_2$	MoS <sub>2</sub> /carbon fibers heterostructure	0.62	1.34	26
	Reduced graphene oxides	$\mathrm{SnO}_2$ quantum dots/S-doped reduced graphene oxides heterostructure	_	2.2-40	78

number of functional groups. Since the functional groups, such as C-OH and C=O groups, have a larger size than atoms, the interlayer spacing is expanded to a greater extent than doping. The expansion range is about 0.1–0.5 nm in this way.

Third, the solvating approach represents the use of solvent molecules to intercalate into the electrode materials and then

expand the interlayer spacing. Using a complex anion with a larger radius, like using AlCl<sub>4</sub><sup>-</sup> to replace Al<sup>3+</sup>, can similarly enlarge the interlayer spacing. The degree of expansion by solvating/using complex anions depends on the size of solvent molecules/complex anions and the number of intercalated molecules/complex anions. In virtue of large size solvent mole-

cules/complex anions, the interlayer spacing can be expanded by 0.2-1.0 nm in most cases.

Fourth, the hierarchical architecture approach refers to mixing different materials to form the electrodes. For example, Wu et al. synthesized SnO2 quantum dots with a diameter of 2.2-3.7 nm and SnO2 nanoparticles with a diameter of about 40 nm to enlarge the interlayer spacing of reduced graphene oxides.<sup>78</sup> In particular, the expansion range of interlayer spacing we count is 0.3-40 nm by compositing hierarchical architectures, which can expand the interlayer spacing by an order of magnitude. From the above, it is believed that interlayer spacing can be expanded by  $10^{-2}$ – $10^{1}$ nm through the selected interlayer engineering method in experiments.

## Conclusion and outlook

To conclude, the graphite anodes have weaker attractions to M ions (Li, Na, and K) when the interlayer spacing of graphite d increases. From the 3D graphite to graphene anode, the  $E_{ad}$  of Li- and Na-ions increase to be positive while that of K-ions is still negative. The enlarged d fails to increase the capacities of Li- and Na-ions but helps increase that of K-ions. Only when  $E_{\rm ad}$  maintains a negative value as d increases, the expanded d of the electrode can increase the capacity. Specifically, the Liion capacity decreases drastically from 372 mA h g<sup>-1</sup> at the equilibrium interlayer spacing  $d_{eq}$  to below 41 mA h g<sup>-1</sup> when d > 4.2 Å; the Na-ion capacity is below 35 mA h g<sup>-1</sup> at any interlayer spacing; the K-ion capacity grows monotonously from 279 mA h g<sup>-1</sup> at its  $d_{eq}$  to 1396 mA h g<sup>-1</sup> at d = 20 Å. Thus, the increase in the capacity of a 2D electrode compared to its bulk counterpart can be predicted by the dependence of  $E_{ad}$  on d. Besides, the storage mechanism shows a tendency from K intercalation to K plating as the number of adsorption layers increases.

The diffusion barriers decrease generally with d and remain still when d is rather large, indicating that the ion-transfer mechanism transforms from bulk diffusion to surface diffusion. Specifically, by increasing d, the electrostatic potential of graphite U becomes smoother, and the ability to buffer the fluctuation of *U* becomes poorer in the M ions. These two effects jointly lead to a minimum of the diffusion barrier of M ions on graphite when  $d_1$  is near its maximum (0.01–0.05 eV), instead of a strictly monotonous decline with d. Based on the design needs, a strategy is put forward to choose the overall optimal d according to the dependence of capacity, ion transfer, and electron transfer on d.

Finally, a set of HT programs have been developed to screen the well-performed anode materials and their optimal interlayer spacing  $d_{\rm op}$  more efficiently. This HT program is expected to be applied more widely. The dependence of d on the performance of other layered anode materials, such as C<sub>2</sub>N<sup>79</sup> and black phosphorus,80 can also be investigated with the above procedures. The relationship between the diffusion barrier and capacity is worth more research. In all, our theoretical findings

can guide interlayer engineering in experiments to choose suitable techniques and achieve the best performance.

## Conflicts of interest

There are no conflicts to declare.

## **Acknowledgements**

This work was supported by the Ministry of Science and Technology of China (No. 2016YFB0700600 (National Materials Genome Project) and 2017YFA206303), the National Natural Science Foundation of China (No. 91964101, 11674005, and 11664026), Open Fund of IPOC (BUPT), the High-performance Computing Platform of Peking University, and the MatCloud+ High Throughput Materials Simulation Platform.

## References

- 1 A. Manthiram, A Reflection on Lithium-ion Battery Cathode Chemistry, Nat. Commun., 2020, 11(1), 1550.
- 2 A. M. Abakumov, S. S. Fedotov, E. V. Antipov and J.-M. Tarascon, Solid State Chemistry for Developing Better Metal-Ion Batteries, Nat. Commun., 2020, 11(1), 4976.
- 3 P. R. Kumar, Y. H. Jung, K. K. Bharathi, C. H. Lim and D. K. Kim, High Capacity and Low Cost Spinel Fe<sub>3</sub>O<sub>4</sub> for Na-Ion Battery Negative Electrode Materials, Electrochim. Acta, 2014, 146, 503-510.
- 4 J. H. Schunemann, H. Dreger, H. Bockholt and A. Kwade, Smart Electrode Processing for Battery Cost Reduction, ECS Trans., 2016, 73(1), 153-159.
- 5 Y. Xue, Q. Zhang, W. Wang, H. Cao, Q. Yang and L. Fu, Two-Dimensional Materials for Energy Conversion and Storage: A Concept, Adv. Energy Mater., 2017, 7(19), 1602684.
- Pomerantseva and Y. Gogotsi, Two-Dimensional Heterostructures for Energy Storage, Nat. Energy, 2017, 2(7),
- 7 J. Liu, S. Wang, Y. Qie, C. Zhang and Q. Sun, High-Pressure-Assisted Design of Porous Topological Semimetal Carbon for Li-ion Battery Anode with High-Rate Performance, Phys. Rev. Mater., 2018, 2(2), 025403.
- 8 L. Peng, Y. Zhu, D. Chen, R. S. Ruoff and G. Yu, Two-Dimensional Materials for Beyond-Lithium-Ion Batteries, Adv. Energy Mater., 2016, 6(11), 1600025.
- 9 D. Wu, B. Yang, H. Chen and E. Ruckenstein, Nitrogenated Holey Graphene C2N Monolayer Anodes for Lithium- and Sodium-Ion Batteries with High Performance, Energy Storage Mater., 2019, 16, 574-580.
- 10 H. Huang, H.-H. Wu, C. Chi, J. Zhu, B. Huang and Out-of-Plane Ion Transport Nitrogenated Holey Graphite A Promising High-Rate Anode for Both Li and Na Ion Batteries, Nanoscale, 2019, 11(40), 18758-18768.

11 F. J. Sonia, M. K. Jangid, M. Aslam, P. Johari and A. Mukhopadhyay, Enhanced and Faster Potassium Storage in Graphene with Respect to Graphite: A Comparative Study with Lithium Storage, ACS Nano, 2019, 13(2), 2190–2204.

Nanoscale

- 12 J. Mei, T. Liao, L. Kou and Z. Sun, Two-Dimensional Metal Oxide Nanomaterials for Next-Generation Rechargeable Batteries, *Adv. Mater.*, 2017, **29**(48), 1700176.
- 13 K. Zhong, R. Hu, G. Xu, Y. Yang, J.-M. Zhang and Z. Huang, Adsorption and Ultrafast Diffusion of Lithium in Bilayer Graphene: Ab Initio and Kinetic Monte Carlo Simulation Study, *Phys. Rev. B*, 2019, **99**(15), 155403.
- 14 L. Cong, H. Xie and J. Li, Hierarchical Structures Based on Two-Dimensional Nanomaterials for Rechargeable Lithium Batteries, *Adv. Energy Mater.*, 2017, 7(12), 1601906.
- 15 K. Share, A. P. Cohn, R. Carter, B. Rogers and C. L. Pint, Role of Nitrogen-Doped Graphene for Improved High-Capacity Potassium Ion Battery Anodes, ACS Nano, 2016, 10(10), 9738–9744.
- 16 Z. Ju, P. Li, G. Ma, Z. Xing, Q. Zhuang and Y. Qian, Few Layer Nitrogen-Doped Graphene with Highly Reversible Potassium Storage, *Energy Storage Mater.*, 2018, **11**, 38–46.
- 17 G. Zou, C. Wang, H. Hou, C. Wang, X. Qiu and X. Ji, Controllable Interlayer Spacing of Sulfur-Doped Graphitic Carbon Nanosheets for Fast Sodium-Ion Batteries, *Small*, 2017, 13(31), 1700762.
- 18 Y. Wen, K. He, Y. Zhu, F. Han, Y. Xu, I. Matsuda, *et al.*, Expanded Graphite as Superior Anode for Sodium-Ion Batteries, *Nat. Commun.*, 2014, 5(1), 4033.
- 19 H. Kim, J. Hong, G. Yoon, H. Kim, K.-Y. Park, M.-S. Park, et al., Sodium Intercalation Chemistry in Graphite, Energy Environ. Sci., 2015, 8(10), 2963–2969.
- 20 A. P. Cohn, K. Share, R. Carter, L. Oakes and C. L. Pint, Ultrafast Solvent-Assisted Sodium Ion Intercalation into Highly Crystalline Few-Layered Graphene, *Nano Lett.*, 2016, 16(1), 543–548.
- 21 G. Yoon, H. Kim, I. Park and K. Kang, Conditions for Reversible Na Intercalation in Graphite: Theoretical Studies on the Interplay Among Guest Ions, Solvent, and Graphite Host, *Adv. Energy Mater.*, 2017, 7(2), 1601519.
- 22 S. C. Jung, Y.-J. Kang and Y.-K. Han, Origin of Excellent Rate and Cycle Performance of Na<sup>+</sup>-Solvent Cointercalated Graphite vs. Poor Performance of Li<sup>+</sup>-Solvent Case, *Nano Energy*, 2017, 34, 456–462.
- 23 M. Goktas, C. Bolli, E. J. Berg, P. Novák, K. Pollok, F. Langenhorst, et al., Graphite as Cointercalation Electrode for Sodium-Ion Batteries: Electrode Dynamics and the Missing Solid Electrolyte Interphase (SEI), Adv. Energy Mater., 2018, 8(16), 1702724.
- 24 X. Xie, Z. Ao, D. Su, J. Zhang and G. Wang, MoS<sub>2</sub>/Graphene Composite Anodes with Enhanced Performance for Sodium-Ion Batteries: The Role of the Two-Dimensional Heterointerface, *Adv. Funct. Mater.*, 2015, 25(9), 1393–1403.
- 25 Y. Jiang, D. Song, J. Wu, Z. Wang, S. Huang, Y. Xu, et al., Sandwich-like SnS<sub>2</sub>/Graphene/SnS<sub>2</sub> with Expanded Interlayer Distance as High-Rate Lithium/Sodium-Ion Battery Anode Materials, ACS Nano, 2019, 13(8), 9100–9111.

- 26 C. Zhao, C. Yu, M. Zhang, Q. Sun, S. Li, M. Norouzi Banis, et al., Enhanced Sodium Storage Capability Enabled by Super Wide-Interlayer-Spacing MoS<sub>2</sub> Integrated on Carbon Fibers, Nano Energy, 2017, 41, 66–74.
- 27 C. Tang, Q. Zhang, M.-Q. Zhao, J.-Q. Huang, X.-B. Cheng, G.-L. Tian, *et al.*, Nitrogen-Doped Aligned Carbon Nanotube/Graphene Sandwiches: Facile Catalytic Growth on Bifunctional Natural Catalysts and Their Applications as Scaffolds for High-Rate Lithium-Sulfur Batteries, *Adv. Mater.*, 2014, 26(35), 6100–6105.
- 28 F. Li, R. Tao, X. Tan, J. Xu, D. Kong, L. Shen, et al., Graphite-Embedded Lithium Iron Phosphate for High-Power-Energy Cathodes, Nano Lett., 2021, 21(6), 2572– 2579.
- 29 G. Kresse and J. Furthmüller, Efficiency of *Ab initio* Total Energy Calculations for Metals and Semiconductors Using a Plane-Wave Basis Set, *Comput. Mater. Sci.*, 1996, **6**(1), 15–50.
- 30 G. Kresse and J. Furthmüller, Efficient Iterative Schemes for Ab Initio Total-Energy Calculations Using a Plane-Wave Basis Set, *Phys. Rev. B: Condens. Matter Mater. Phys.*, 1996, 54(16), 11169–11186.
- 31 J. P. Perdew, K. Burke and M. Ernzerhof, Generalized Gradient Approximation Made Simple, *Phys. Rev. Lett.*, 1996, 77(18), 3865–3868.
- 32 J. P. Perdew, J. A. Chevary, S. H. Vosko, K. A. Jackson, M. R. Pederson, D. J. Singh, et al., Atoms, Molecules, Solids, and Surfaces: Applications of the Generalized Gradient Approximation for Exchange and Correlation, Phys. Rev. B: Condens. Matter Mater. Phys., 1992, 46(11), 6671–6687.
- 33 J. Yang, R. Quhe, S. Liu, Y. Peng, X. Sun, L. Zha, *et al.*, Gatetunable high magnetoresistance in monolayer Fe<sub>3</sub>GeTe<sub>2</sub> spin valves, *Phys. Chem. Chem. Phys.*, 2020, 22(44), 25730–25739.
- 34 C. Yang, Z. Song, X. Sun and J. Lu, Valley Pseudospin in Monolayer MoSi<sub>2</sub>N<sub>4</sub> and MoSi<sub>2</sub>As<sub>4</sub>, *Phys. Rev. B*, 2021, **103**(3), 035308.
- 35 P. E. Blöchl, Projector Augmented-Wave Method, *Phys. Rev. B: Condens. Matter Mater. Phys.*, 1994, **50**(24), 17953–17979.
- 36 S. Grimme, J. Antony, S. Ehrlich and H. Krieg, A Consistent and Accurate Ab Initio Parametrization of Density Functional Dispersion Correction (DFT-D) for the 94 Elements H-Pu, J. Chem. Phys., 2010, 132(15), 154104.
- 37 L. Xu, S. Liu, H. Zhang, X. Zhang, J. Li, J. Yan, *et al.*, First-Principles Simulation of Monolayer Hydrogen Passivated Bi<sub>2</sub>O<sub>2</sub>S<sub>2</sub>-Metal Interfaces, *Phys. Chem. Chem. Phys.*, 2020, 22(15), 7853–7863.
- 38 G. Henkelman and H. Jónsson, Improved Tangent Estimate in the Nudged Elastic Band Method for Finding Minimum Energy Paths and Saddle Points, *J. Chem. Phys.*, 2000, **113**(22), 9978–9985.
- 39 G. Henkelman, B. P. Uberuaga and H. Jónsson, A Climbing Image Nudged Elastic Band Method for Finding Saddle Points and Minimum Energy Paths, *J. Chem. Phys.*, 2000, 113(22), 9901–9904.

- 40 Z. Song, X. Sun and L. Wang, Switchable Asymmetric Moiré Patterns with Strongly Localized States, J. Phys. Chem. Lett., 2020, 11(21), 9224-9229.
- 41 J. Ma, R. Quhe, Z. Zhang, C. Yang, X. Zhang, J. Li, et al., Two-dimensional materials as stabilized interphase for solid-state electrolyte Li<sub>10</sub>GeP<sub>2</sub>S<sub>12</sub> in lithium metal batteries, J. Mater. Chem. A, 2021, 9, 4810-4821.
- 42 X. Yang, Z. Wang, X. Zhao, J. Song, C. Yu, J. Zhou, et al., MatCloud, a High-Throughput Computational Materials Infrastructure: Present, Future Visions, and Challenges, Chin. Phys. B, 2018, 27(11), 110301.
- 43 X. Yang, Z. Wang, X. Zhao, J. Song, M. Zhang and H. Liu, MatCloud: High-Throughput Computational Infrastructure for Integrated Management of Materials Simulation, Data and Resources, Comput. Mater. Sci., 2018, 146, 319-333.
- 44 N. Yabuuchi, K. Kubota, M. Dahbi and S. Komaba, Research Development on Sodium-Ion Batteries, Chem. Rev., 2014, 114(23), 11636-11682.
- 45 R. Shannon, Revised Effective Ionic Radii and Systematic Studies of Interatomic Distances in Halides Chalcogenides, Acta Crystallogr., Sect. A: Cryst. Phys., Diffr., Theor. Gen. Crystallogr., 1976, 32(5), 751-767.
- 46 C. Yang, X. Sun, X. Zhang, J. Li, J. Ma, Y. Li, et al., Is Graphite Nanomesh a Promising Anode for the Na/K-Ions Batteries?, Carbon, 2020, 176, 242-252.
- 47 E. Hazrati, G. A. de Wijs and G. Brocks, Li Intercalation in Graphite: A van der Waals Density-Functional Study, Phys. Rev. B: Condens. Matter Mater. Phys., 2014, 90(15), 155448.
- 48 E. Lee and K. A. Persson, Li Absorption and Intercalation in Single Layer Graphene and Few Layer Graphene by First Principles, Nano Lett., 2012, 12(9), 4624-4628.
- 49 K. Nobuhara, H. Nakayama, M. Nose, S. Nakanishi and H. Iba, First-Principles Study of Alkali Metal-Graphite Intercalation Compounds, J. Power Sources, 2013, 243, 585-587.
- 50 E. Ziambaras, J. Kleis, E. Schröder and P. Hyldgaard, Potassium Intercalation in Graphite: A van der Waals Density-Functional Study, Phys. Rev. B: Condens. Matter Mater. Phys., 2007, 76(15), 155425.
- 51 C. Niu, H. Pan, W. Xu, J. Xiao, J.-G. Zhang, L. Luo, et al., Self-Smoothing Anode for Achieving High-Energy Lithium Batteries under Realistic Conditions, Nanotechnol., 2019, 14(6), 594-601.
- 52 S. M. Girvin and K. Yang, Modern Condensed Matter Physics, Cambridge University Press, Cambridge, 2019.
- 53 X. Fan, W. T. Zheng and J.-L. Kuo, Adsorption and Diffusion of Li on Pristine and Defective Graphene, ACS Appl. Mater. Interfaces, 2012, 4(5), 2432-2438.
- 54 K. C. Wasalathilake, G. A. Ayoko and C. Yan, Effects of Heteroatom Doping on the Performance of Graphene in Sodium-Ion Batteries: A Density Functional Theory Investigation, Carbon, 2018, 140, 276-285.
- 55 J. Yang, Y. Yuan and G. Chen, First-Principles Study of Potassium Adsorption and Diffusion on Graphene, Mol. Phys., 2020, 118(1), e1581291.

- 56 F. J. Sonia, M. K. Jangid, B. Ananthoju, M. Aslam, P. Johari and A. Mukhopadhyay, Understanding the Li-Storage in Few Layers Graphene with Respect to Bulk Graphite: Experimental, Analytical and Computational Study, J. Mater. Chem. A, 2017, 5(18), 8662-8679.
- 57 X. Zhang, C. Yang, Y. Pan, M. Weng, L. Xu, S. Liu, et al., Monolayer GaS with High Ion Mobility and Capacity as A Promising Anode Battery Material, J. Mater. Chem. A, 2019, 7(23), 14042-14050.
- 58 C. Yang, X. Zhang, J. Li, J. Ma, L. Xu, J. Yang, et al., Holey Graphite: A Promising Anode Material with Ultrahigh Storage for Lithium-Ion Battery, Electrochim. Acta, 2020, 346, 136244.
- 59 C. Eames and M. S. Islam, Ion Intercalation into Two-Dimensional Transition-Metal Carbides: Global Screening for New High-Capacity Battery Materials, J. Am. Chem. Soc., 2014, 136(46), 16270–16276.
- 60 H. Fujimoto, M. Fujimoto, H. Ikeda, R. Ohshita, S. Fujitani and I. Yonezu, Electrochemical Characteristics of Lithiated Graphite (LiC<sub>6</sub>) in PC Based Electrolytes, J. Power Sources, 2001, 93(1), 224-229.
- 61 D. Datta, J. Li, N. Koratkar and V. B. Shenoy, Enhanced lithiation in defective graphene, Carbon, 2014, 80, 305-310.
- 62 K. Kim, Z. Lee, W. Regan, C. Kisielowski, M. F. Crommie and A. Zettl, Grain Boundary Mapping in Polycrystalline Graphene, ACS Nano, 2011, 5(3), 2142-2146.
- 63 P. Y. Huang, C. S. Ruiz-Vargas, A. M. van der Zande, W. S. Whitney, M. P. Levendorf, J. W. Kevek, et al., Grains and Grain Boundaries in Single-layer Graphene Atomic Patchwork Quilts, Nature, 2011, 469(7330), 389-392.
- 64 H. I. Rasool, C. Ophus, W. S. Klug, A. Zettl and J. K. Gimzewski, Measurement of the Intrinsic Strength of Crystalline and Polycrystalline Graphene, Nat. Commun., 2013, 4(1), 2811.
- 65 P. Ge and M. Fouletier, Electrochemical Intercalation of Sodium in Graphite, Solid State Ionics, 1988, 28-30, 1172-1175.
- 66 D. A. Stevens and J. R. Dahn, The Mechanisms of Lithium and Sodium Insertion in Carbon Materials, J. Electrochem. Soc., 2001, 148(8), A803.
- 67 Y. Liu, B. V. Merinov and W. A. Goddard, Origin of Low Sodium Capacity in Graphite and Generally Weak Substrate Binding of Na and Mg among Alkali and Alkaline Earth Metals, Proc. Natl. Acad. Sci. U. S. A., 2016, 113(14), 3735-3739.
- 68 H. Moriwake, A. Kuwabara, C. A. J. Fisher and Y. Ikuhara, Why Is Sodium-Intercalated Graphite Unstable?, RSC Adv., 2017, 7(58), 36550-36554.
- 69 H. Kim, J. Hong, Y.-U. Park, J. Kim, I. Hwang and K. Kang, Sodium Storage Behavior in Natural Graphite using Etherbased Electrolyte Systems, Adv. Funct. Mater., 2015, 25(4), 534-541.
- 70 X.-F. Luo, C.-H. Yang, Y.-Y. Peng, N.-W. Pu, M.-D. Ger, C.-T. Hsieh, et al., Graphene Nanosheets, Carbon Nanotubes, Graphite, and Activated Carbon as Anode

Nanoscale Paper

- Materials for Sodium-Ion Batteries, J. Mater. Chem. A, 2015, 3(19), 10320–10326.
- 71 A. Ramos, I. Cameán, N. Cuesta and A. B. García, Is Single Layer Graphene A Promising Anode for Sodium-Ion Batteries?, *Electrochim. Acta*, 2015, **178**, 392–397.
- 72 Z. Jian, W. Luo and X. Ji, Carbon Electrodes for K-Ion Batteries, *J. Am. Chem. Soc.*, 2015, **137**(36), 11566–11569.
- 73 M. Kühne, F. Börrnert, S. Fecher, M. Ghorbani-Asl, J. Biskupek, D. Samuelis, *et al.*, Reversible Superdense Ordering of Lithium between Two Graphene Sheets, *Nature*, 2018, **564**(7735), 234–239.
- 74 J. B. Goodenough and Y. Kim, Challenges for Rechargeable Li Batteries, *Chem. Mater.*, 2010, 22(3), 587–603.
- 75 J. Ma, J. Fu, M. Niu and R. Quhe, MoO<sub>2</sub> and Graphene Heterostructure as Promising Flexible Anodes for Lithium-Ion Batteries, *Carbon*, 2019, **147**, 357–363.
- 76 Q. Zhang, J. Ma, M. Lei and R. Quhe, Metallic MoN Layer and its Application as Anode for Lithium-Ion Batteries, *Nanotechnology*, 2018, **29**(16), 165402.
- 77 F. Wu, R. Dong, Y. Bai, Y. Li, G. Chen, Z. Wang, *et al.*, Phosphorus-Doped Hard Carbon Nanofibers Prepared by Electrospinning as an Anode in Sodium-Ion Batteries, *ACS Appl. Mater. Interfaces*, 2018, **10**(25), 21335–21342.
- 78 K. Wu, B. Shi, L. Qi, Y. Mi, B. Zhao, C. Yang, et al., SnO<sub>2</sub> Quantum Dots @ 3D Sulfur-Doped Reduced Graphene Oxides as Active and Durable Anode for Lithium Ion Batteries, Electrochim. Acta, 2018, 291, 24–30.
- 79 Y. Ding, C. You, Y. Xu, L. Zhong, Q. Deng, J. Li, et al., Stability and reaction thermodynamics of boron-doped nitrogenated holey graphene (NHG) monolayers and their energy storage properties for Li, Na and K-ion batteries: A

- first principles investigation, Appl. Surf. Sci., 2021, 559, 149849.
- 80 S. M. Atashzar, S. Javadian, H. Gharibi and Z. Rezaei, Defective phosphorene as an anode material for high-performance Li-, Na-, and K-ion batteries: a first-principles study, *Nanoscale*, 2020, **12**(39), 20364–20373.
- 81 F. Niu, J. Yang, N. Wang, D. Zhang, W. Fan, J. Yang, et al., MoSe<sub>2</sub>-Covered N,P-Doped Carbon Nanosheets as a Long-Life and High-Rate Anode Material for Sodium-Ion Batteries, *Adv. Funct. Mater.*, 2017, 27(23), 1700522.
- 82 Y.-X. Wang, S.-L. Chou, H.-K. Liu and S.-X. Dou, Reduced Graphene Oxide with Superior Cycling Stability and Rate Capability for Sodium Storage, *Carbon*, 2013, 57, 202–208.
- 83 A. P. Vijaya Kumar Saroja, M. Muruganathan, K. Muthusamy, H. Mizuta and R. Sundara, Enhanced Sodium Ion Storage in Interlayer Expanded Multiwall Carbon Nanotubes, *Nano Lett.*, 2018, **18**(9), 5688–5696.
- 84 M.-C. Lin, M. Gong, B. Lu, Y. Wu, D.-Y. Wang, M. Guan, et al., An Ultrafast Rechargeable Aluminium-Ion Battery, *Nature*, 2015, **520**(7547), 324–328.
- 85 Y. Liang, H. D. Yoo, Y. Li, J. Shuai, H. A. Calderon, F. C. Robles Hernandez, *et al.*, Interlayer-Expanded Molybdenum Disulfide Nanocomposites for Electrochemical Magnesium Storage, *Nano Lett.*, 2015, 15(3), 2194–2202.
- 86 C. Zhao, X. Wang, J. Kong, J. M. Ang, P. S. Lee, Z. Liu, et al., Self-Assembly-Induced Alternately Stacked Single-Layer MoS<sub>2</sub> and N-doped Graphene: A Novel van der Waals Heterostructure for Lithium-Ion Batteries, ACS Appl. Mater. Interfaces, 2016, 8(3), 2372–2379.